Sensors and Materials, Vol. 36, No. 4 (2024) 1627–1635
MYU Tokyo

S & M 3622

Damage and Defect Identification in Cementitious Materials with Heat Generation by Applying Sonic-IR Method

Katsufumi Hashimoto,* Nao Takahashi, and Shunsuke Kumagai

Graduate School of Engineering, Hokkaido University, A4-08, N13 W8, Kita-ku, Sapporo 060-8628, Japan

(Received October 20, 2023; accepted April 12, 2024)

Keywords: Sonic-IR, cementitious material, crack, NDT

Accurate and easy-to-use nondestructive tests (NDTs) are strongly required to detect damage and defects in concrete structures. In the Sonic-IR method, the IR radiation due to ultrasonic vibration at the object surface is visualized using a thermography camera. A temperature rise occurs with frictional heat generation due to the rubbing action of crack interfaces. Meanwhile, it is known that the technique is usually introduced for steel and composite materials, which have much higher thermal conductivity than a cement-hardened body. In this study, we applied the Sonic-IR method to identify crack propagation in cementitious materials. We found that the Sonic-IR method can be utilized for detecting the cracks in mortar under compressive stress failure. The resolution for detecting cracks in the targeted specimens was compared between the Sonic-IR method and cross-sectional imaging by X-ray computed tomography (CT) as NDTs. The effective test conditions for evaluating the internal/surface crack by the Sonic-IR method were clarified by changing the ultrasonic vibration frequency and the external force applied to mortar specimens to induce crack formation by compression loading. Varying the testing conditions in the Sonic-IR method, such as stress constraint and ultrasonic frequency, also enabled us to quantitatively observe the fracture progress upon the application of stepwise loading, which causes the evolution of compression failure.

1. Introduction

The performance and safety of aging structures must be ensured through testing, which requires labor and time.[1–3] The management administrators for tunnels and bridges are obliged to assess material and structural performance by nondestructive testing (NDT), which contributes to the appropriate inspection, monitoring, and maintenance required for safety purposes in the use of those social infrastructures.[4–6] In targeting materials such as metals and composites that have higher thermal conductivity than a cement-hardened body, a crack/flaw that appears and evolves with rising temperature can be imaged by infrared thermography under ultrasonic excitation [hereinafter referred to as the Sonic-IR method (Sonic-IR)].[7–9] When continuous vibration with ultrasonic excitation is applied to high-thermal-conductivity materials, the temperature at cracks locally increases owing to the friction and rubbing action of the crack

*Corresponding author: e-mail: hashimoto.k@eng.hokudai.ac.jp
https://doi.org/10.18494/SAM4720

ISSN 0914-4935

interfaces under compressive stress.[10–12] When ultrasonic vibration of an appropriate frequency is applied, frictional heat at the damaged area in a solid body is generated by the clapping and rubbing of the crack interfaces.[13] In demonstrating the heat generation at the region with damage and defects, the sensitivity of an infrared imaging technique depends on the frequency selected for ultrasonic vibration.[13–15] Concrete and mortar, which are cement-based materials, have low thermal conductivity, and the internal conditions depend on their in-service environments in a real situation. However, there are yet no research cases in which Sonic-IR has been applied to cementitious materials for detecting internal cracks.

Referring to the infrared radiation principle, in this study, we investigate the technical procedure with noncontact temperature measuring technology and infrared sensors to visualize the crack interface in cementitious materials. Sonic-IR is introduced to cementitious material (mortar) in this study. Although the testing procedure has been widely used for metals or composites, the applicability of Sonic-IR to cement-hardened materials, which are major construction materials, is unclear, and there are only a few research works on them since their thermal conductivity is comparably low.[16] To investigate the validity of the suitable methodology, the ultrasonic excitation equipment in Sonic-IR, which is normally employed in conventional tests for metals or composites, is introduced to cracked mortar in this study. The objective of this study is to clarify the influence of the mechanical vibration conditions, such as frequency and uniaxial force, on temperature rise when Sonic-IR is applied for detecting the interior crack in mortar. In particular, the rate of temperature change and the area of temperature rise on the target surface were examined for detectable heat generation using an infrared camera. We aim to examine the heat generation behavior and the testing conditions in Sonic-IR for detecting cracks in cement-mortar specimens loaded with uniaxial compressive stress.

2. Sample Preparation

Mortar specimens were prepared with a water–cement ratio (W/C) of 0.5 and sand–cement ratio (S/C) of 3.0. Ordinary Portland cement and standard sand specified in Japanese Industrial Standards (JIS R 5201) were used. Mortar specimens with 50 mm diameter and 100 mm height were prepared. After curing for 28 days in water, the compression test was performed on the cylindrical mortar specimen, the compressive strength of which was 27.6 MPa (n = 3). The damaged (crack-induced) specimens prepared for Sonic-IR are shown in Fig. 1.

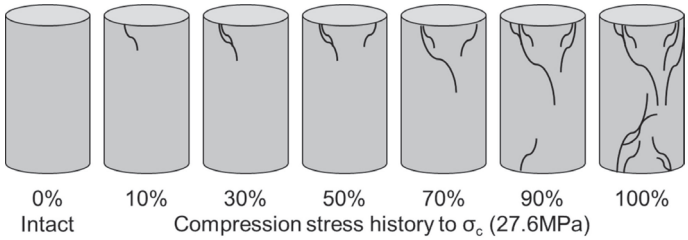

Fig. 1. Mortar specimens with various compression stresses.

The specimens were applied with loads of up to 10, 30, 50, 70, 90, and 100% of the compressive strength to fabricate specimens with different degrees of cracking (damage). The samples loaded to 70 and 90% of compressive strength (hereinafter referred to as the 70% specimen and the 90% specimen, respectively) were used for the investigation in this study.

3. Sonic-IR

Sonic-IR is the imaging technique of frictional heat generated by the rubbing of the contact surfaces of the internal cracks or the crack interfaces. When ultrasonic vibration is excited and propagated through the targeted object, the cracks and the interfaces are identified from the temperature rise due to heat generation displayed in the thermal image obtained using the infrared camera. Several crack imaging methods that combine infrared thermography and ultrasonic excitation (vibration) are referred to as Sonic-IR or vibro-thermography.[17,18] Since these methods utilize heat generation and temperature rise due to the friction between crack surfaces caused by ultrasonic excitation, this technique is suitable for material interface imaging when contact and closure of crack surfaces are expected.[19,20] To detect anomalies accompanied by the propagation of cracks in rocks under external loads, the ultrasonic vibration load test of cylindrical granite samples with 200 N force is carried out using a 30 kHz piezoelectric ceramic ultrasonic vibrator.[21]

Figure 2 shows the testing equipment of Sonic-IR assembled with an ultrasonic excitation system with a stainless-steel horn. The induced ultrasonic excitation frequencies were 20.2 and 28.8 kHz. The displacements of the horn head contacting the top surface of the specimen were a 0.20 μm peak-to-peak amplitude for 20.2 kHz frequency and a 0.15 μm peak-to-peak amplitude for 28.8 kHz frequency. To eliminate the mechanical influence of ultrasonic excitation as much as possible on the cement-hardened body, continuous ultrasonic excitation on the surface of the targeted specimen was implemented for 3 s. The uniaxial load under confined conditions of the vibration horn was set at three levels: 33, 66, and 99 N. Room temperature in the experiment was set at 20 ℃ in an air-conditioned environment. Styrene boards were installed around the

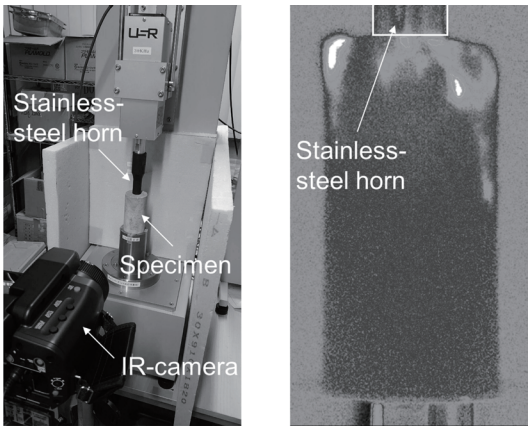

Fig. 2. Experimental setup of and thermal image obtained by Sonic-IR.

specimen for insulation. In the constant-temperature and constant-humidity (R.H. 40%) chamber, the specimens were stored and dried before implementing Sonic-IR.

The distance between the center of the specimen and the camera lens was set at 270 mm. The specimen location was adjusted to horizontally capture the target centered in the detected image. The thermal image recording frame rate was 10 Hz. The thermal images were taken from the front and back of each specimen to obtain the average temperature rise over the whole surface. The surface temperature rise was imaged in 400 pixels × 200 pixels on the target specimen of 50 mm (diameter) × 100 mm (height). Differential analysis of temperature change was performed with reference to the duration of ultrasonic vibration. Under ultrasonic vibration excitation for 3 s, the temperature change in the defined area was calculated as T_1 from 0 to 1 s, T_2 from 0 to 2 s, and T_3 from 0 to 3 s.

The acquired 16-bit X-ray computed tomography (CT) continuous images with the resolution of 37.73 μm/pixel were processed into 8-bit images. The temperature data of the thermal image and the coordinates of the cross-sectional image subjected to 8-bit processing were derived to identify the heat source (internal crack) location and the crack width. By using the plot profile function of ImageJ, two inflection points were identified in the curve showing the change in brightness (gray-scale value) for cracks in the acquired 8-bit image, and the crack width was calculated from the difference in the gray-scale values.

4. Results and Discussion

The total number of pixels in the defined area for the differential thermal analysis in each specimen was used to calculate the ratio of pixels ($P_{0.9}$) where $T_3 > 0.9$ °C, and the averaged values of $P_{0.9}$ for front and back surfaces were obtained from each specimen.

Figure 3 shows $P_{0.9}$ when the frequency of ultrasonic excitation was 20.2 kHz. Figure 4 shows $P_{0.9}$ when the frequency was 28.8 kHz. No heat generation can be confirmed for the intact specimen under any conditions of confined force and ultrasonic vibration frequency. With the applied ultrasonic frequency of 20.2 kHz, heat generation is unclear for the 70% specimen, whereas it becomes marked for the 90% specimen as the confined force increases. On the other

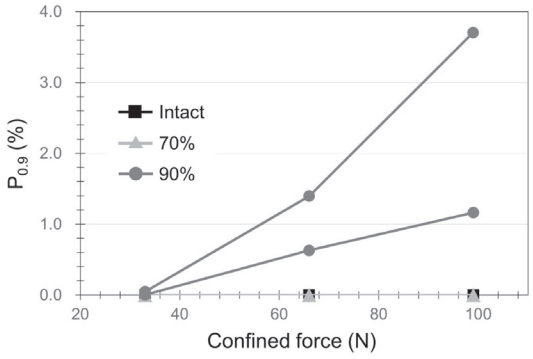

Fig. 3. Ratio of pixels of $P_{0.9}$ ($\Delta T_3 > 0.9$) with 20.2 kHz.

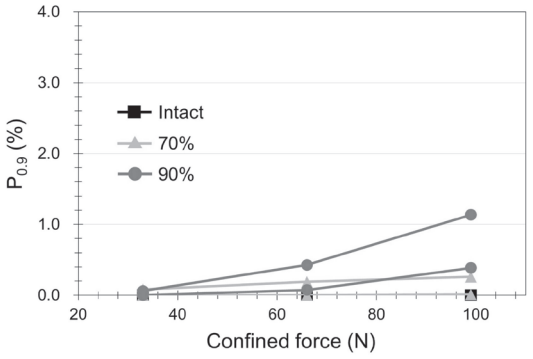

Fig. 4. Ratio of pixels of $P_{0.9}$ ($\Delta T_3 > 0.9$) with 28.8 kHz.

hand, with the applied ultrasonic frequency of 28.8 kHz, slight heat generation in the 70% specimen is observed, while the heat generation in the 90% specimen is reduced in comparison with the case of applying 20.2 kHz ultrasonic vibration.

Generally, the number of internal cracks increases with the increase of loading stress in compression tests.[22,23] Therefore, it is considered that the heat generation due to frictional action is likely to occur with an increase in the number of internal cracks. It can be seen that the 90% specimen displays more extensive and intense heat generation than does the 70% specimen. The result indicates that the progress of damage with crack formation can be detected with greater heat generation in the case of 20.2 kHz than in that of 28.8 kHz.

Figure 5 shows the calculated result of the ratio of pixels ($P_{0.5}$), where $T_3 > 0.5$ °C for the 70% specimen. Although no significant heat generation is observed in Figs. 3 and 4, it is confirmed that the heat generated with 28.8 kHz ultrasonic excitation is greater than that with 20.2 kHz ultrasonic excitation for the 70% specimen, unlike the 90% specimen. From the above results, it is found that there is a difference in the heat generation behavior examined with Sonic-IR depending on the degree of damage. Furthermore, the ultrasonic excitation frequency and the confining force on the specimen affect the frictional heat behavior at the crack. In the compression test, it is known that the width of the crack usually increases with increasing uniaxial load.[22,23] This suggests that there is a certain correlation between the frequency of ultrasonic excitation and the width of the crack detected by Sonic-IR in cementitious materials.

Figure 6 shows an X-ray CT image of a cross section in the 70% specimen. The temperature profiles on the surface at 5 mm from the top are detected by Sonic-IR, as shown in Figs. 7 and 8 for 20.2 and 28.8 kHz ultrasonic excitation, respectively. The results were obtained under the confined force of 99 N. The results indicate that the heat generation behavior not observable with 20.2 kHz excitation can be seen with 28.8 kHz excitation in zone A. This indicates that there are defects such as microcracks that can be detected only with 28.8 kHz excitation. However, no cracks are visually confirmed in the cross-sectional X-ray CT image at the location where the heat generation is identified. In compression tests for concrete, it was revealed in previous studies that microcracks of less than 0.1 mm width occur inside the specimen even when only 70% of the compressive strength is applied.[23] Therefore, it is considered that the 70% specimens

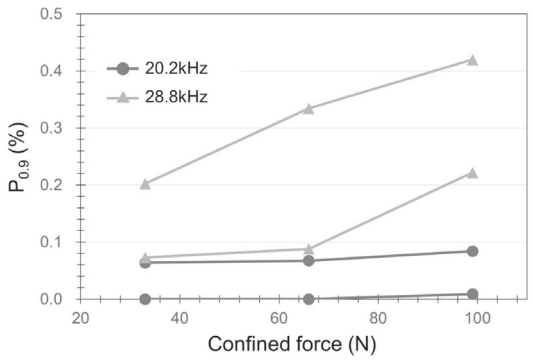

Fig. 5. Ratio of pixels of $P_{0.9}$ ($\Delta T_3 > 0.9$) for 70% specimen.

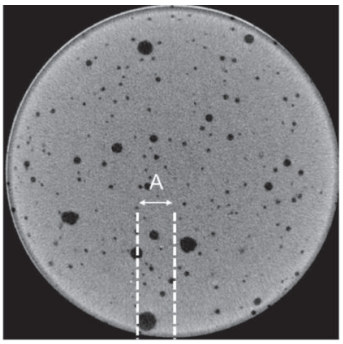

Fig. 6. X-ray CT image of 70% specimen at 5 mm from the top.

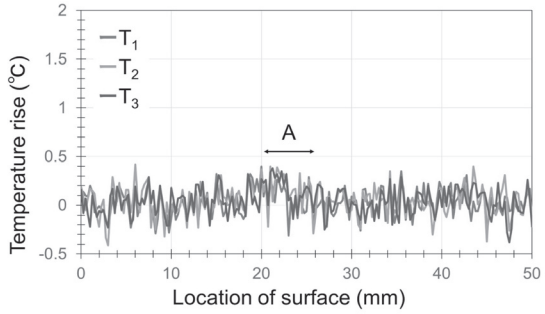

Fig. 7. Temperature rise with 20.2 kHz on 70% specimen surface.

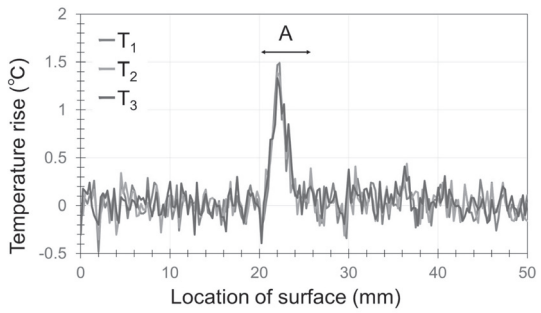

Fig. 8. Temperature rise with 28.8 kHz on 70% specimen surface.

in this study contain only microcracks. This implies that microcracks that cannot be visualized in X-ray CT images with a resolution of 37.73 μm/pixel can be detected in the thermal images obtained by Sonic-IR with 28.8 kHz ultrasonic excitation.

Figure 9 shows an X-ray CT image of a cross section in the 90% specimen. The temperature profiles on the surface at 5 mm from the top can be detected by Sonic-IR, as shown in Fig. 10, with 20.2 kHz ultrasonic excitation since the heat generation is obvious (see Figs. 3 and 4). The results were obtained under the confined force of 99 N.

In the cross-sectional image shown in Fig. 9, it is confirmed that cracks exist at the point corresponding to zone B, where heat generation is indicated by the sharp peak in the line profile in Fig. 10, and the crack width is 0.25 mm. In zones C and D of the cross section shown in Fig. 9, the crack width could not be clearly observed (measured) because of the insufficient resolution of the X-ray CT image. However, heat generation is observed by Sonic-IR, as shown in Fig. 10, in zones C and D. On the other hand, although the crack visualized in zone E is detected to be 0.36 mm in width, the heat generation is quite small, as shown in Fig. 10.

Figure 11 shows the changes in the rate of temperature change V (°C/s) with time from 0 to 1 s, 1 to 2 s, and 2 to 3 s when the ultrasonic excitation frequency was 28.8 kHz for cracks in zone A of the 70% specimens (Fig. 6) and 20.2 kHz for cracks in zone E of the 90% specimens (Fig. 9). A large temperature rise from 0 to 1 s and the stagnation of heat generation from 1 to 3 s is seen for the invisible crack in zone A. For the detected (visualized) crack of 0.36 mm width in zone E at 5 mm from the top, the crack width is 0.34 mm at 10 mm and 0.31 mm at 15 mm from the top of the specimen (ultrasonic excitation point). The cross-sectional images are shown in Figs. 12 and 13, respectively. The rates of temperature rise are also indicated in Fig. 11.

When the surface opening crack widths are 0.36 and 0.34 mm, a constant temperature rise is observed from 0 to 1 s and 1 to 2 s, and the heat generation gradually stagnates from 2 to 3 s. When the crack opening width is 0.31 mm, the temperature increases significantly from 0 to 1 s, but remains stagnant from 1 to 2 and 2 to 3 s. It is additionally confirmed that the surface temperature increases upon applying ultrasonic vibration for 3 s are 0.74 °C for 0.36 mm, 0.90 °C for 0.34 mm, and 1.67 °C for 0.31 mm crack opening widths. Therefore, from the above-described results, it is found that crack closure may generate frictional heat effectively depending on the excitation frequency of ultrasonic vibration.

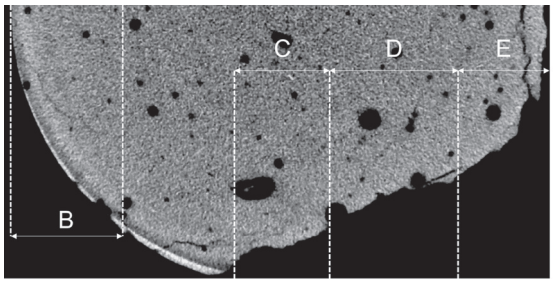

Fig. 9. X-ray CT image of 90% specimen at 5 mm from the top.

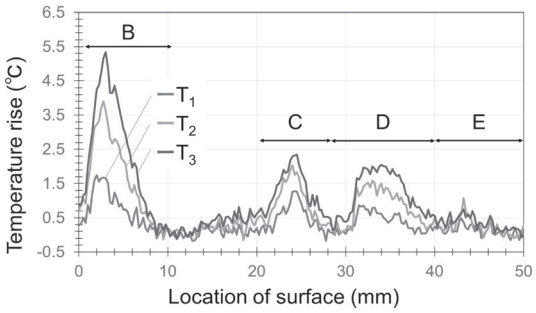

Fig. 10. Temperature rise with 20.2 kHz on 90% specimen.

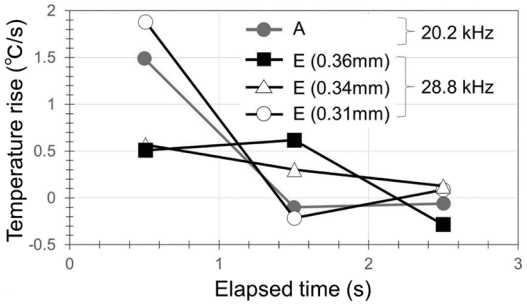

Fig. 11. Rate of temperature rise with 20.2 and 28.8 kHz.

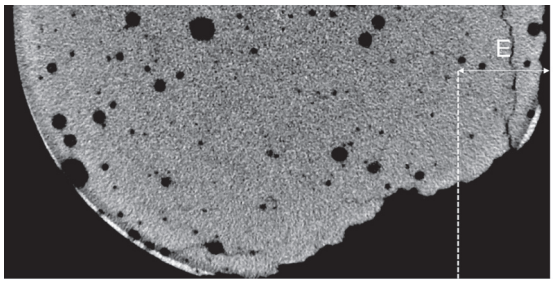

Fig. 12. X-ray CT image of 90% specimen at 10 mm from the top.

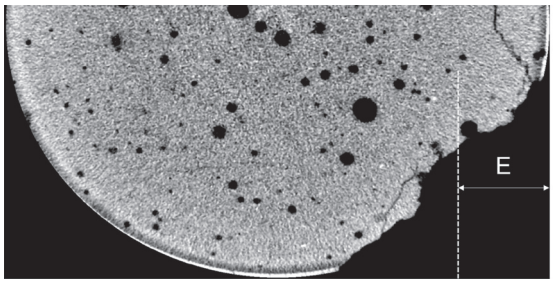

Fig. 13. X-ray CT image of 90% specimen at 15 mm from the top.

5. Conclusions

As one of the noncontact sensor technologies, infrared thermography enables crack detection in cementitious materials under ultrasonic vibration. By applying Sonic-IR to mortar specimens, crack propagation subjected to different compressive stress histories was evaluated, and the following findings were obtained.

1) The degree of damage in mortar influences the effects of the restraining force and the frequency of the ultrasonic vibration on the heat generation behavior.
2) Sonic-IR can detect microscopic cracks propagated in the cement matrix, which cannot be identified or visualized in X-ray CT images.
3) There is a correlation between the rate of temperature change (°C/s) upon ultrasonic excitation and the opening width of the crack.

References

1 fib Bulletin 93: Birth Certificate and Through-life Management Documentation (fib, Switzerland, 2020). https://doi.org/10.35789/fib.BULL.0093
2 J. Matos, A. Solgaard, C. Santos, M. S. Silva, P. Linneberg, A. Strauss, J. Casas, C. Caprani, and M. Akiyama: Proc. 2017 fib Conf. (2018) 1832–1839. https://doi.org/10.1007/978-3-319-59471-2_210
3 H. Yokota and K. Hashimoto: Int. J. Struct. Eng. **4** (2013) 138. https://doi.org/10.1504/IJSTRUCTE.2013.050770
4 S. Lee and N. Kalos: J. Civ. Eng. Manage **21** (2015) 654. https://doi.org/10.3846/13923730.2014.890665
5 ACI Committee 228: Report on Nondestructive Test Methods for Evaluation of Concrete in Structures (American Concrete Institute, 2013). https://www.concrete.org/portals/0/files/pdf/previews/228213.pdf
6 R. Wan-Wendner: J. Land Manage. Food and Environ. **69** (2018) 175. https://doi.org/10.2478/boku-2018-0015
7 R. B. Mignogna, R.E. Green Jr, J. C. Duke Jr, E. G. Henneke II, and K. L. Reifsnider: Ultrasonics **7** (1991) 159. https://doi.org/10.1016/0041-624X(81)90095-0
8 L. H. Tenek and E. G. Henneke: Proc. SPIE 1467 (The International Society for Optical Engineering, 1991) 252–263. https://doi.org/10.1117/12.46440
9 X. P. V. Maldague: Mater. Eval. **60** (2002) 1060. http://www.123seminarsonly.com/Seminar-Reports/012/67084371-Introduction-to-NDT-by-Active-Infrared-Thermography1.pdf
10 J. Renshaw, S. D. Holland, R. B. Thompson, and C. Uhl: AIP Conf. Proc. **1096** (2009) 473. https://dr.lib.iastate.edu/server/api/core/bitstreams/71370e27-68c6-432c-a64d-bf688e20b20f/content
11 J. Lu, X. Han, G. Newaz, L. D. Favro, and R. L. Thomas: Nondestruct. Test. Eval. **22** (2007) 127. https://doi.org/10.1080/10589750701448175
12 D. Imanishi and Y. Nishina: Adv. Exp. Mech. **6** (2021) 47. https://doi.org/10.11395/aem.6.0_47
13 G. P. M. Fierro, D. Calla', D. Ginzburg, F. Ciampa, and M. Meo: J. Sound Vib. **404** (2017) 102. https://doi.org/10.1016/j.jsv.2017.05.041
14 Q. Yu, O. Obeidat, and X. Han: AIP Conf. Proc. **2102** (2019) 120001. https://doi.org/10.1063/1.5099843
15 W. Guo, L. Dong, H. Wang, Z. Xing, F. Feng, Z. Gao, and B. Wang: Infrared Phys. Technol. **102** (2019) 103073. https://doi.org/10.1016/j.infrared.2019.103073
16 K. Hashimoto and T. Shiotani: Constr. Build. Mater. **386** (2023) 131549. https://doi.org/10.1016/j.conbuildmat.2023.131549
17 X. Maldague and S. Marinetti: J. Appl. Phys. **79** (1996) 2694. https://doi.org/10.1063/1.362662
18 L. D. Favro, X. Han, Z. Ouyang, G. Sun, H. Sui, and R. L. Thomas: Rev. Sci. Instrum. **71** (2000) 2418. https://doi.org/10.1063/1.1150630
19 M. Matsushita-Tokugawa, J. Miura, Y. Iwami, T. Sakagami, Y. Izumi, N. Mori, M. Hayashi, S. Imazato, F. Takeshige, and S. Ebisu: J. Endod. **39** (2013) 88. https://doi.org/10.1016/j.joen.2012.06.033
20 X. Han, L. D. Favro, Z. Ouyang, and R. L. Thomas: J. Adhes. **76** (2001) 151. https://doi.org/10.1080/00218460108029622
21 D. Zhao, S. Zhang, Y. Zhao, and M. Wang: Environ. Earth Sci. **78** (2019) 1. https://doi.org/10.1007/s12665-019-8450-6
22 S. Hong,P. Liu, J. Zhang, F. Xing, and B. Dong: Cem. Concr. Compos. **100** (2019) 15. https://doi.org/10.1016/j.cemconcomp.2019.03.010
23 Y. Obara, I. Tanikura, J. Jung, R. Shintani, and S. Watanabe: J. Adv. Concr. Technol. **14** (2016) 433. https://doi.org/10.3151/jact.14.433

About the Authors

Katsufumi Hashimoto received his B.S., M.S., and Ph.D. degrees from Tokyo Institute of Technology, Japan, in 2005, 2007, and 2010, respectively. From 2011 to 2016, he was an assistant professor at Hokkaido University, Japan. From 2016 to 2021, he was a senior lecturer and an associate professor at Kyoto University, and since 2021, he has been an associate professor at Hokkaido University. His research interests are in construction materials and structural evaluation for inspection and monitoring using nondestructive testing (NDT) methods. (hashimoto.k@eng.hokudai.ac.jp)

Nao Takahashi received his B.S. degree from Hokkaido University, Japan, in 2022. Since 2022, he has been a master's course student in graduate school at Hokkaido University, Japan. His research interest is in the application of Sonic-IR for cementitious materials. (t_nao_pokudai0220@eis.hokudai.ac.jp)

Shunsuke Kumagai received his B.S. degree from Hokkaido University, Japan, in 2023. Since 2023, he has been a master's course student in graduate school at Hokkaido University, Japan. His research interest is in the application of Sonic-IR for cementitious materials. (kuma624shi@eis.hokudai.ac.jp)